CrystEngComm

Accepted Manuscript

ROYAL SOCIETY OF CHEMISTRY

www.rsc.org/crystengcomm

A simple and efficient synthetic route for preparation of $NaYF_4$ upconversion nanoparticles by thermo-decomposition of rare-earth oleates

Xiaodong Liu[1,2], Xiao Zhang[2,4], Gan Tian[2,3*], Wenyan Yin[2], Liang Yan[2], Longfei Ruan[2], Zhiyong Yang[5], Debao Xiao[1,*] and Zhanjun Gu[2,*]

[1]College of Environmental and Chemical Engineering, Yanshan University, Qinhuangdao, 066004, P. R. China

[2] Key Laboratory for Biomedical Effects of Nanomaterials and Nanosafety, Institute of High Energy Physics, Chinese Academy of Sciences, Beijing 100049, P. R. China.

[3] College of Chemistry, Sichuan University, Chengdu, 610064, P. R. China

[4] Key Lab oratory for Biomedical Effects of Nanomaterials and Nanosafety, National Center for Nanosciences and Technology of China, Beijing, 100190, China

[5]School of Chemistry and Chemical Engineering, University of Chinese Academy of Sciences

*Correspondence: tiangan@ihep.ac.cn, debao.xiao@ysu.edu.cn, zjgu@ihep.ac.cn,

Abstract

Hexagonal-phase $NaYF_4$ nanocrystals with well uniformity and monodispersity have been successfully achieved through a thermal decomposition of rare-earth oleate complexes. By co-doping upconverters (Yb/Er, Yb/Tm or Yb/Ho) or downconverters (Eu or Ce/Tb), multicolor upconversion (UC) luminescence under 980-nm laser excitation or downconversion luminescence under UV irradiation could be obtained. For the first time, we systematically investigate the effects under various parameters including reaction temperature, time, NaF to rare-earth ions ratio and oleic acid concentration on their size, morphology, phase purity and UC emission properties using Yb/Er co-doped $NaYF_4$ UC nanoparticles as the typical example. The results demonstrated this strategy is a simple yet efficient way for fabrication of UCNPs with well uniformity and monodispersity, which enriches the synthetic routes for production of high quality hexagonal-phase $NaYF_4$ nanocrystals. In addition, a mesoporous silica layer was coated onto the hydrophobic $NaYF_4$:Yb/Er nanoparticles and converted them into hydrophilic ones, which then could be performed as a potential luminescent probe for cell imaging and a promising nanocarrier for therapeutic drug delivery, making them as a multifunctional platform for simultaneous imaging and therapy.

1. Introduction

Rare-earth upconversion nanoparticles (UCNPs) are luminescent nanophosphors that could convert the low-energy photon excitation into the higher energy light

emission through a multiphoton absorption process.[1] Such unique luminescence property endows them with many special advantages as alternative luminescent probes to conventional labels, because the near infrared radiation (NIR)source minimizes the light-induced autofluorescence and photodamage to bio-tissue as well as enables high penetration depth in biospecies. In addition, these UCNPs are featured with strong resistance to photobleaching, high chemical stability and low toxicity.[2-5] As a result, a great deal of research efforts have been devoted on synthesis and surface-modification of UCNPs for using as luminescent probes in biological labeling and imaging technology.

As an ideal host material, the rare-earth fluorides with high refractive index and low phonon frequency have aroused intensive research in the past few decades.[6-12] So far, Yb/Er or Yb/Tm co-doped $NaYF_4$ nanocrystals are recognized as the most efficient 980-nm NIR-to-visible upconverting materials and hexagonal phase $NaYF_4$ (β-$NaYF_4$) offers about an order of magnitude enhancement of upconversion efficiency relative to its cubic phase counterpart.[7, 10] Therefore, β-$NaYF_4$ has been increasingly chosen as the host matrix for upconversion.[10-13] Several chemical approaches including coprecipitation and hydrothermal synthesis have been adopted to synthesize β-$NaYF_4$-based UCNPs. However, coprecipitation methods usually require an annealing treatment to improve crystallinity of the products, and hydrothermal approaches typically involve prolonged reaction time. Moreover, these methods usually suffer from its low yield and the as-synthesized products show poor uniformity and dispersibility.[14, 15] Yan et al and Chow et al pioneered the synthesis of

large-scaled β-$NaYF_4$ UCNPs via the thermal decomposition of corresponding trifluoroacetate precursors in organic solvents medium with high boiling points. Nonetheless, various toxic fluorinated and oxyfluorinated carbon species are simultaneously generated by the pyrolysis of trifluoroacetates, which has become the matters of substantial environmental concern.[16] Zhang et al developed a novel solvothermal route to synthesize pure hexagonal-phase $NaYF_4$:Yb/Er(Tm) nanocrystals using RE chlorides, NaOH and NH_4F as raw materials.[17] In this strategy, small solid-state crystal nuclei formed at the earlier stage would be ripened when reaction temperature increases. However, the multiple heating up-cooling downing-heating up steps are complicated and time/power-consuming. In addition, the co-solvent methanol must be completely removed, otherwise, the products are irregular shaped and weak-luminescent. Thus, the discovery and exploitation of a facile, environment-friendly and effective mass production approach to synthesize *β*-$NaYF_4$-based nanocrystals with well-defined shapes and good dispersibility should have great potential.

Recently, a two-step thermo-decomposition route using rare-earth oleate as precursor has been widely adopted for the synthesis of various rare-earth oxides.[18] Unfortunately, few reports focused on the rare-earth fluorides obtained from this class of precursor. Actually, oleates as precursor for synthesis of rare-earth fluorides based UCNPs are pretty much environmental friendly and have distinctive advantages over the above-mentioned precursors. Unlike the trifluoroacetates, no toxic side-products would be produced during the thermo-decomposition of oleate precursors; on the

other hand, oleates precursors could be well dissolved in OA/ODE media, where the toxic co-solvent, such as methanol, is no longer needed, and the procedure is facile compared with RE chlorides precursor based approach. As far as we know, a detailed investigation/report for researchers on controllable synthesis of high-quality and monodispersed β-$NaYF_4$-based luminescent nanophosphors has never been presented. In this work, we employ the rare-earth oleates and NaF as the precursors to synthesize β-$NaYF_4$:Yb/Er UCNPs, and for the first time, systematically investigate the influence factors including NaF to Y^{3+} ratio, reaction time and temperature, oleic acid concentration and OA/ODE ratio and then point out the optimized synthetic parameters for the fabrication of high-quality and well-dispersed UCNPs based on the comprehensive consideration of size, morphology, crystal phase purity and luminescent property. The products are well characterized by XRD, SEM, FT-IR and upconversion luminescence (PL) spectra, respectively. The obtained OA-capped nanocrystals are readily dissolved in cyclohexane to form a stable colloidal solution. Moreover, surface modifications of the as-prepared hydrophobic β-$NaYF_4$:Yb/Er UCNPs were performed to convert them into hydrophilic ones that can be well-dispersed in aqueous solutions for potential biological applications.[19-23]

2. Experimental section

Materials. $Y(NO_3)_3·6H_2O$ (99.90%), $Yb(NO_3)_3·5H_2O$ (99.90%), $Er(NO_3)_3·6H_2O$ (99.90%), $Tm(NO_3)_3·xH_2O$ (99.90%, x≈5), $Ho(NO_3)_3·5H_2O$ (99.90%), $Eu(NO_3)_3·6H_2O$ (99.90%), $Ce(NO_3)_3·6H_2O$ (99.90%), $Tb(NO_3)_3·xH_2O$ (99.90%,

x≈6), 1-octadecene (ODE, 90%), oleic acid (OA, 99%) and tetraethylorthosilicate (TEOS) were obtained from Alfa Aesar Reagent Company. Sodium oleate (98.0%) was purchased from Aladdin Chemical Co. and ammonium nitrate was provided by Sigma-Aldrich. Doxorubicin (DOX, 99%) was adapted from Beijing HuaFeng United Technology CO., Ltd. NaF, NaOH, ethanol and cyclohexane were supplied by Beijing Chemical Reagent Company. All the chemicals were of analytical grade and used without further purification. Deionized water was used in all experiments.

Synthesis of Rare-Earth Oleate Complexes. In a typical procedure for yttrium-oleate complex preparation, yttrium nitrate (20 mmol) and sodium oleate (60 mmol) were dissolved in a mixture solvent consisted of distilled water (30 mL), ethanol (40 mL) and hexane (70 mL). The resultant solution was put into a 250 mL flask and then stirred vigorously for 12 h at room temperature. After that, the reaction solution was moved into a separatory funnel. The upper organic layer was separated from the mixture and washed with deionized water/absolute ethanol (1:1 v/v) three times. The final product was obtained in a waxy solid form by rotary evaporation and then dispersed in a mixture of oleic acid and 1-octadecene for further use. Other rare-earth oleate complexes were prepared in the same way.

Synthesis of $NaYF_4$: Yb/Er Upconversion Nanoparticles. In a typical process, 0.336 g (8 mmol) of NaF, 0.78 mmol of yttrium-oleate complex, 0.2 mmol of yttrbium-oleate complex, 0.02 mmol of erbium-oleate complex were added into a 50

mL single-neck flask containing a certain amount of oleate acid and 1-octadecene. The mixture was heated at 130 ºC to promote the dissolution of NaF for 45 min under vigorous stirring. After that, the mixture was degassed and then kept at 300 ºC for 1 h in argon atmosphere under vigorous stirring. When the reaction solution was cooled to room temperature, 10 mL of ethanol was added into the flask to precipitate the products. After that, the mixture was centrifuged and washed for 2～3 times with ethanol. Finally, the as-prepared nanoparticles were dispersed and stored in cyclohexane.

A similar process was adopted to synthesize $NaYF_4$: Yb/Tm (20/0.5 mol%), $NaYF_4$: Yb/Tm/Er (20/0.5/0.2 mol%), $NaYF_4$: Yb/Ho (20/2 mol%) upconversion nanoparticles and $NaYF_4$: Eu (5 mol%), $NaYF_4$: Ce/Tb (20/5 mol%) downconversion nanocrystals.

Surface Modification. Mesoporous silica coating was employed to transfer these hydrophobic OA-capped UCNPs (OA-UCNPs) into hydrophilic ones according a previously reported literature.[24] The OA-UCNPs dispersed in 2 mL of cyclohexane solution (5 mg mL^{-1}) was added dropwise in the mixture of 0.1 g of CTAB and 20 mL of water. The mixture solution was heated to 75 ºC under vigorously stirring to evaporate cyclohexane. After the appearance of a transparent solution, 10 mL of CTAB stabilized UCNPs solution was added to a mixed solution containing 20 mL of water, 3 mL of ethanol and 150 μL of 2 M NaOH, and then the mixture was heated up to 70 ºC under stirring. 150 μL of tetraethylorthosilicate (TEOS) was added dropwise

and the reaction was maintained for 10 min. The obtained nanoparticles were centrifuged and washed with ethanol several times. After that, the CTAB molecules were removed via ion exchange method as followed:[25] The last-step products were transferred into a mixture of 50 mL of ethanol and 0.3 g of NH_4NO_3, kept at 60 ºC for 2 h, and then dispersed in ethanol to get the final product with mesoporous silica shell (UCNPs@mSiO_2).

Cytotoxicity Assay. A standard Cell Counting Kit-8 (CCK-8) colorimetric assay was employed to evaluate the potential cytotoxicity of UCNPs@mSiO_2 in Hela cells. In a typical experiment, the Hela cells were seeded into a 96-well culture plate (5000/well) and cultured at 37 ºC and 5% CO_2 for 12 h. UCNPs@mSiO_2 with different concentrations were diluted in DMEM, placed into the cells, and incubated for another 12 or 24 h at 37 ºC. After efficient PBS washing, the CKK-8/DMEM solution was put into wells and the cells were cultured for additional 2 h. The absorbance at 450 nm was measured on a microplate reader (Multiskan MK3, Thermo Scientific). The cell viability was calculated as the following formula:

Cell viability (%) = (mean of Abs value of treatment group/mean of Abs value of control) × 100.

For evaluating the DOX cell killing ability, the Hela cells were plated out in a 96-well culture plate (5000/well) and cultured for 24 h. A series of concentrations of free DOX or DOX-UCNPs@mSiO_2 were placed into the cells, and incubated for 1 h, and then changed to CKK-8/DMEM solution after washing. With further 2 h

incubation, the cell viability was determined by measuring the absorbance.

In vitro Cell Imaging. Hela cells (2×10^5) were planted on a confocal dish with DMEM supplemented with 10% Fetal Bovine Serum (FBS) for 24 h. 1mL of 100 μg/mL UCNPs@$mSiO_2$ dispersed in DMEM were added to the dish and the cells was incubated at 37 ºC and 5% CO_2 for another 2 h. After that, PBS was employed to wash out the unbound nanoparticles. Meanwhile, the cells cultured with UCNPs@$mSiO_2$ were imaged in bright field and under NIR excitation using an inverted fluorescence microscope equipped with 980 nm laser excitation.

Preparation of drug storage and delivery system. For the loading of DOX on the UCNPs@$mSiO_2$ (DOX-UCNPs@$mSiO_2$), the procedure is that 5 mg of the UCNPs@$mSiO_2$ nanoparticles dispersed in a 10 mL solution of DOX in phosphate buffer solution (PBS, pH 7.4) stirring for 24 h under dark condition. Typically, a certain amount of UCNPs@$mSiO_2$ sample were immersed in different concentrations (100～1200 μM) of DOX solution. After stirring for 24 h at room temperature, the DOX loaded samples were collected by centrifugation at 12000 rpm for 8 minutes and then freeze-dried under vacuum for 12 h. The amount of released DOX was measured by UV-vis spectrophotometer at a wavelength of 480 nm between original and final DOX solution.

To evaluate the DOX-released efficiency, 20 mg of UCNPs@$mSiO_2$ samples were immersed in 10 mL PBS solution (pH = 5.0 or 7.4) at 37 ºC under continuous stirring.

At predetermined time intervals, 3 ml of the released medium was taken and centrifuged. The supernatant solution was determined to obtain the residual DOX content by UV-vis measurement. Finally, the intake of medium was returned to the original released medium.

Characterization. The morphology and size of the as-synthesized nanoparticles were characterized by the field emission scanning electron microscope (FE-SEM, Hitachi, S-4800) and transmission electron microscope (TEM, Tecnai G2 20 S-TWIN operated at 200 kV). Powder X-ray diffraction (XRD) patterns of the dried products were measured using a Japan Rigaku D/max-2500 diffractometer with $Cu_{k\alpha}$ radiation (λ=1.5418Å). The photoluminescence spectra were obtained by a fluorescence spectrophotometer (Horiba Jobin Yvon FluorolLog3) with a xenon lamp and an external 980 nm laser. All photos of upconversion luminescence were acquired by a Nikon D3100 digital camera. Fourier Transform infrared (FT-IR) spectra were carried out by a Fourier transform Bruker EQUINOX55 spectrometer with the KBr pellet technique.

3. Results and discussion

The process of the preparation of $NaYF_4$:Yb/Er(20/2 mol%) nanoparticles was adopted by a liquid-solid two-phase strategy. However, the synthesis of nanocrystals could be constrained by many experimental conditions, such as reaction temperature, time, reactants concentration and the type and the amount of solvent, thereby affecting the nanoparticles' morphology, size, crystal phase and fluorescence properties, etc. In

this study, we have been conducted a basic and detailed investigation as follows.

3.1 Effect of the Reaction Temperature

To investigate the effect of reaction temperature on the synthesis of upconversion nanoparticles, different reaction temperatures (260 ºC, 280 ºC, 300 ºC, 320 ºC) were used to study its influence on morphological **(Figure 1a-d)** and structural properties of the nanocrystals. The XRD patterns of the as-prepared $NaYF_4$:Yb/Er(20/2 mol%) nanoparticles at different temperature were shown in **Figure 1e**. For the product synthesized at 260 ºC, the major species were cubic phase with a small quantity being hexagonal phase, and the size of nanoparticles was less than 10 nm (**Figure 1a**). With the increased temperature, the samples transformed from cubic to hexagonal phase remarkably, as shown in **Figure 1e**. Meanwhile, nanocrystals with broad size distributions were received, which could be attributed to nucleation and growth of nanoparticles (**Figure 1b**). The pure hexagonal $NaYF_4$:Yb/Er was achieved when the temperature reached 300 ºC and no distinct extra diffraction peaks were observed even the temperature increased to 320 ºC (see **Figure 1e**). Moreover, ca. 22 nm hexagonal-phase nanoparticles with a narrow size distribution were synthesized **(Figure 1c)**. For the temperature at 320 ºC, the obtained samples had a slight increase in size （the average diameter is about 25 nm ）**(Figure 1d)**. The fluorescence intensity of upconversion were enhanced obviously with increasing reaction temperature **(Figure 1f)**, which were in accordance with the nanoparticles' size and crystal phase evolution. Consequently, it was reasonable to choose 300 ºC as the

reaction temperature to product the mono-dispersed nanoparticles.

3.2 Effect of the Reaction Time

The reaction time also played a key role in preparation of $NaYF_4$ nanoparticles (**Figure 2**). **Figure 2e** showed that the XRD patterns of the nanoparticles synthesized at 300 ºC at different reaction time. When the reaction time is 0.5 h, a great mass of samples were hexagonal phase with a small amount being cubic phase. With increasing the reaction time to 1 h, the pure hexagonal $NaYF_4$ was received. This result indicated that the phase transformation from cubic to hexagonal phase occurred with the extension of reaction time. With further prolonging the reaction time, no cubic $NaYF_4$ phase could be detected anymore and only hexagonal phase existed.

Figure 2 showed FE-SEM image of $NaYF_4$:Yb/Er (20/2 mol%) nanoparticles obtained at 300 ºC for various reaction periods. In the initial period, at t=0.5 h, SEM image (**Figure 2a**) revealed that various size of nanoparticles less than 15 nm were obtained, which could be ascribed to the beginning of nucleation and growth of nanoparticles. Correspondingly, the relatively weak fluorescence intensity was observed in **Figure 2f.** With the reaction holding on for 1 h, the mono-dispersed and uniform $NaYF_4$ nanoparticles with an average size of 23 nm and a narrow size distribution were produced **(Figure 2b)**. When the reaction time was prolonged to 1.5 h (**Figure 2c**) or 2 h (**Figure 2d**), as-prepared nanoparticles had no apparent changing in size and morphology. Moreover, as shown in **Figure 2f** , the fluorescence intensity did not obviously change, which was consistent with the size of the nanoparticles.

Accordingly, it is optimal to take 1 h as the reaction time in this work.

3.3 Effect of varying the Molar Quantities of NaF

The size, shape and crystal structure of the as-produced $NaYF_4$ nanoparticles have been researched by altering the content of NaF from 4 mmol to 12 mmol. Under the constant reaction conditions, the synthesized nanocrystals with different sizes were obtained in the stoichiometric proportion of NaF: RE^{3+} (RE=sum of the rare-earth ions). SEM image (**Figure 3a**) indicated that the as-prepared $NaYF_4$ nanocrystals were composed of a small amount of spherical nanoparticles with several nanometers and large quantity of hexagonal nanoprisms with an average of 55 nm in diameter and 45nm in thickness. Accordingly, as-presented X-ray diffraction pattern of the samples could be attributed to a mixture of the hexagonal and cubic phase, as shown in **Figure 3e**. With the ratio reached 6, that is, the NaF exceeded RE^{3+} slightly, and the produced nanocrystals were composed of uniform and mono-dispersed hexagonal nanoparticles with an average diameter of 30 nm (**Figure 3b**). Meanwhile, the XRD pattern confirmed the disappearance of cubic phase and occurrence of a direction cubic to hexagonal phase conversion facilitated by addition of NaF. Furthermore, with further increasing ratio up to 8 or 12, regular nanoparticles with the average diameter about 25 nm were produced and no distinct size or morphology difference was observed (see **Figure 3c,d**). The XRD pattern of the nanoparticles with pure hexagonal phase observed in the **Figure 3e** was well-demonstrated that the NaF content has no effect on nanocrystal phase.

Figure 3f showed the upconversion fluorescence spectra of the $NaYF_4$: Yb/Er (20/2 mol%), which were synthesized with varying NaF: RE^{3+} ratios under the settled conditions. As the content of NaF increased, the average size of the as-prepared nanocrystals decreased gradually, resulting in the weaker outcome the intensity of upconcversion emission. The fact that the intensity of upconcversion emission decreased with the increase NaF content was assigned to different surface states of nanocrystals with various sizes.[26] Moreover, this result also suggested that the intensity of upconversion fluorescence was demonstrated morphology and size dependence.

3.4 Effect of the Ligand

The ligand, such as oleic acid, have large influence on the produced $NaYF_4$ nanoparticles. Here, the preliminary study on the size and morphology of the prepared nanoparticles by changing the relative content of the oleic acid was proceeded. Setting the total volume of the ligands including OA and ODE for 21 mL, 6 ml oleic acid was added in the system while other parameters containing *t*=1 h, T=300 ºC and 8 mmol NaF were kept constant. SEM image in **Figure 4a** showed that some irregular and large $NaYF_4$ nanocrystals were achieved, including nanoparticles and nanorods. With extending the content of OA to 9 ml, slightly small nanocrystals of an average 33 nm in diameter were obtained (**Figure 4b**). When an excess amount of OA (11 mL or 15 mL) was added, it was found that the size of as-prepared nanoparticles tended to decrease gradually (**Figure 4c,d**). The results indicated that the content of OA had a

great impact on the growth of the $NaYF_4$ nanocrystals. As known, the RE ions could be readily coordinated with the carboxylic groups, thus the OA molecules working as the chelating agent were absorbed on the growing lanthanide nanocrystals and leaded to delay the growth rate of the nanoparticles. With constant addition the amount of OA, the smaller nanoparticles were gained. The results from the XRD patterns in **Figure 4e** showed that there were no differences in crystalline phases when various amount of OA were added in the system. Only the pure hexagonal phase of as-produced nanoparticles was found with increasing the content of OA, which could be ascribed to the reaction under a high temperature and long time. The dependence of the up-conversion fluorescence intensity on the size of the $NaYF_4$ nanocrystals was observed clearly in **Figure 4f**. By fixing other reaction conditions, as more OA was added, the nanoparticles size tended to become smaller. Furthermore, the intensity of the up-conversion nanocrystals decreased gradually along with their smaller sizes.

3.5 Multicolor fluorescence Emission

In order to investigate fluorescence emission properties of the as-prepared nanocrystals, various luminescent RE ions (Ho^{3+}, Tm^{3+}, Tm^{3+}/Er^{3+}, Eu^{3+}, Ce^{3+}/Tb^{3+}) were doped in $NaYF_4$ nanoparticles, thus the upconversion and downcoversion luminescence were observed in our experiment. The UC emission spectra of the as-synthesized $NaYF_4$: Yb/Ho (20/2 mol%) dispersed in hexane were measured under 980 nm laser diode excitation and presented in **Figure 5a**. There were two weak red emissions centered at 648, 658 nm and one strong green emission centered at 540 nm.

The red emission peaks were assigned to the results of transitions from $^5F_5$ to $^5I_8$, and the green emission was caused by the $^5S_2 \rightarrow {}^5I_8$ of Ho^{3+}. Consequently, the green emission output could be observed (**Figure 5f**). For the $NaYF_4$: Yb/Tm (20/0.5 mol%) nanocrystals, the main ultra-violet emission at about 360 nm was ascribed to the transition from $^1D_2$ to $^3H_6$ of Tm^{3+}. Other emission bands, such as, centered at about 450, 476, 646 and 698 nm were assigned to $^1D_2 \rightarrow {}^3F_4$, $^1G_4 \rightarrow {}^3H_6$, $^1G_4 \rightarrow {}^3F_4$, and $^3F_3 \rightarrow {}^3H_6$ of Tm^{3+} transitions, respectively. The strong near-to-infrared emission at about 800 nm corresponded to the transition from $^3H_4$ to $^3H_6$ of Tm^{3+}. Therefore, bright blue emission could be observed by a digital photograph in **Figure 5g**. For a three-component doped system for $NaYF_4$: Yb/Er/Tm(20/0.2/0.5 mol%) upconversion nanoparticles, the emission peaks of Er^{3+} were observed in the visible spectral region except for Tm^{3+}, as shown in **Figure 5c**. There were four emission centers at about 409, 521, 539, and 654 nm , which could be attributed to $^2H_9 \rightarrow {}^4I_{15/2}$, $^2H_{11/2} \rightarrow {}^4I_{15/2}$, $^4S_{3/2} \rightarrow {}^4I_{15/2}$ and $^4F_{9/2} \rightarrow {}^4I_{15/2}$ transitions of Er^{3+} ions, respectively. Meanwhile, a digital photograph from the **Figure 5h** exhibited strong white emission under excitation.

The DC emission of the $NaYF_4$ nanocrystals was investigated in detail to demonstrate multicolor fine-tuning in the visible region. In the cased of $NaYF_4$: Eu (5 mol%), **Figure 5d** shows the emission spectra of the products upon excitation at 254 nm. The emission bands centered at 583, 591, 615, 649 and 694 nm are generated from the $^5D_0 \rightarrow {}^7F_0$, $^5D_0 \rightarrow {}^7F_1$, $^5D_0 \rightarrow {}^7F_2$, , $^5D_0 \rightarrow {}^7F_3$ and , $^5D_0 \rightarrow {}^7F_4$ transitions of Eu^{3+} ions, respectively. Moreover, a strong red emission was observed under

ultraviolet light excitation, which could be presented by the digital photograph (see the **Figure 5i**). For the $NaYF_4$: Ce/Tb (20/5 mol%) nanoparticles, the as-prepared simples emitted bright-green light under ultraviolet light excitation (**Figure 5j**). The characteristic emission bands centered at 488, 542, 583 and 622 nm were observed from the emission spectra, which originated from the $^5D_4 \rightarrow {}^7F_6$, $^5D_4 \rightarrow {}^7F_5$, $^5D_4 \rightarrow {}^7F_4$ and $^5D_4 \rightarrow {}^7F_3$ transition of Tb^{3+} ions, respectively. The most prominent group was derived from $^5D_4 \rightarrow {}^7F_5$ transition, which resulted in a strong green emission.

3.6 Surface modification, cytotoxicity evaluation and Bio-imaging

It is noteworthy that the UCNPs possessing unique optical properties have broad applications in biological field. For UCNPs to be successfully used as luminescent labels, they must exhibit good water-solubility. Silica coating is a well-established strategy for surface modification of UCNPs.[27-31] Monodisperse spherical-like OA-capped $NaYF_4$:Yb/Er (denoted as OA-$NaYF_4$:Yb/Er) with an average diameter of about 30 nm (**Figure 6a**) were treated by a modified Stöber procedure for the formation of the composites with a mesoporous silica layer. The UCNPs@mSiO_2nanoparticles have obviously larger size at about 50 nm and the core–shell structure can be clearly distinguished because of the different electron penetrability between the cores and shells (**Figure 6b**). The hydrophilic UCNPs@mSiO_2 could be readily dispersed in DI Water and form a nearly transparent solution (**Figure 6c inset**). Compared with OA-capped UCNPs dispersed in cyclohexane, the emission intensity of the UCNPs@mSiO_2 in DI water have a mild

decline, which arises from the water that has high vibrational energy causing an increase in the multi-phonon relaxation in the aqueous media, as shown **Figure 6c.**

With regard to their potential application as bioprobes in bioimaging, it is necessary to evaluate the cytotoxicity of these nanoparticles. The cytotoxicity of the UCNPs@$mSiO_2$ nanoparticles was initially estimated by a standard Cell Counting Kit-8 (CCK-8) colorimetric assay with Hela cells. As shown in **Figure 6d**, there are no significant differences in cell viability in the range of 0-400 μg mL^{-1} and the viability of Hela cells was greater than 90 % after 12 or 24 h incubation even at the highest concentration of 400 μg mL^{-1}. On the basis of the above-presented cytotoxicity results, it can be deduced that the hydrophilic UCNPs@$mSiO_2$ are biocompatible and nontoxic to living cells, and could serve as probes for cell imaging. Further practical application of in upconversion luminescence imaging was investigated by utilizing an inverted microscope equipped with a CW excitation at 980 nm. Hela cells were incubated in a serum-free medium containing UCNPs@$mSiO_2$ (50 μg/mL) at 37 ºC for 2 h and the unattached NPs were removed by PBS washing. As shown in **Figure 6(e-g)**, obvious green luminescent emission under 980-nm excitation was observed and no autofluorescence signal could be found in the UCL image of Hela cells **(Figure 6f)**. The overlay of the bright-field and UCL **(Figure 6g)** indicated that these NPs existed in the cells, indicating they could be used as luminescent labels for biological imaging.

3.7 Drug loading/release behavior and in vitro cell treatment study

It is commonly known that mesoporous silica possess excellent drug storage and sustained drug release properties.[32-34] In our experiment, doxorubicin (DOX) was chosen as the model drug to evaluate the loading capability and release behaviors of the UCNPs@$mSiO_2$ nanocarries. As seen in the **Figure 7a**, the DOX loading amount trend was concentration-dependent and saturated at about 1000 μM with the saturated capacity at 0.156 mmol/g, which could be determined by the characteristic DOX absorbance change peaked at ～480 nm (**Figure 7b**). The in vitro release profiles of DOX from DOX-load UCNPs@$mSiO_2$ (DOX-UCNPs@$mSiO_2$) nanoparticles over a 24 h period in PBS buffer solution at two different pH values was shown in **Figure 7c**. The drug release rate of DOX-UCNPs@$mSiO_2$ was remarkably pH-dependent and increased gradually upon decreasing pH. In neutral PBS (pH 7.4) to simulate normal physiological conditions, only 23% DOX was released from DOX-UCNPs@$mSiO_2$ composite. With an increase of acidity to pH 5.0, to simulate the intracellular conditions of cancer cells, the release rate of DOX became much faster and over 70% DOX was released from the composite. The pH-sensitive DOX released from nanoparticles might be beneficial for controlled drug delivery and release into cancer cells since the microenvironments in intracellular lysosomes, endosomes and certain cancerous tissues was acidic.[35] To demonstrate the cancer killing ability, the Hela cells were respectively incubated with free DOX and DOX-UCNPs@$mSiO_2$ nanoparticles for 24 h with equivalent DOX concentrations. As presented in **Figure 7d**, the drug-loaded nanoparticles could obviously cause cytotoxicity to Hela cells. More importantly, DOX-UCNPs@$mSiO_2$ nanoparticles exhibited better efficacy in

these cases. The enhanced efficacy may be ascribed to the fact that the more DOX-UCNPs@mSiO$_2$ nanoparticles can be taken up by Hela cells than when using free DOX alone, which results in releasing more DOX molecules inside to induce cell death. Based on these results, the UCNPs@mSiO$_2$ can potentially be employed as a vehicle for drug loading and delivery in cancer therapy.

4. Conclusions

To sum up, systematic investigation and manipulation of the morphology and size of hexagonal-phase $NaYF_4$ nanocrystals with well uniformity and monodispersity have been successfully achieved using a simple, efficient and environmentally benign strategy based on thermal decomposition of rare-earth oleate complexes. The effects of reaction temperature, time, NaF and oleic acid concentration, on the size, morphology and crystal phase purity of the β-$NaYF_4$ have been investigated in details. Thorough and detailed characterization results indicated the oleate precursor could be developed as a promising candidate to enrich the preparation techniques for hexagonal-phase $NaYF_4$ nanocrystals. Due to the desirable hexagonal phase, bright multicolor UC and DC luminescence could be achieved. The as-obtained spherical nanocrystals were also modified to have hydrophilic surface by mesoporous silica coating, and further applied for in vitro bio-imaging and drug delivery, demonstrating the multifunctionality of the as-prepared UCNPs.

Acknowledgements

This work was supported by National Basic Research Programs of China (973 program, No. 2012CB932504, 2011CB933403 and 2012CB934001), and National Natural Science Foundation of China (No. 21177128, 21171122 21101158，and 21303200).

References

1 M. Haase and H. Schäfer, *Angew. Chem, Int. Ed.*, 2011, **50**(26), 5808-5829.

2 D. Jin, J. A. Piper, *Anal. Chem.*, 2011, **83**(6), 2294-2300.

3 L. J. Zhou, Z. J. Gu, X. X. Liu, W. Y. Yin, G. Tian, L. Yan, S. Jin, W. L. Ren, G. M. Xing, W. Li, X. L. Chang, Z. B. Hu and Y. L. Zhao, *J. Mater. Chem.*, 2012, **22**(3), 966-974.

4 R. Kumar, M. Nyk, T. Y. Ohulchanskyy, C.A. Flask and P. N. Prasad, *Adv. Funct. Mater.*, 2009, **19**(6), 853-859.

5 Y. M. Yang, F. Liu, X. G. Liu and B. G. Xing, *Nanoscale*, 2013, **5**(1), 231-238.

6 J. F. Suyver, J. Grimm, M. K.van Veen, D. Biner, K. W. Kramer and H. U.Gudel, *J. Lumin.*, 2006, **117**(1),1-12.

7 Y. W. Zhang, X. Sun, R. Si, L. P. You, C. H. Yan, *J. Am. Chem. Soc.*, 2005, **127**(10), 3260-3261.

8 H. X. Mai, Y. W. Zhang, R. Si, Z. G. Yan, L. S. Sun, L. P. You, C. H. Yan, *J. Am. Chem. Soc.*, 2006, **128**(19), 6426-6436.

9 F. Wang, D. K. Chatterjee, Z. Q. Li, Y. Zhang, X. P. Fan, M. Q. Wang, *Nanotechnology*, 2006, **17**(23), 5786.

10 Y. X. Liu, D. S. Wang, J. X. Shi, Q. Peng and Y. D. Li, *Angew. Chem. Int. Ed*, 2013, **52**(16), 4366-4369.

11 Z. J. Gu, L. Yan, G. Tian, S. J. Li, Z. F. Chai and Y. L. Zhao, *Adv. Mater.*, 2013, **25**(28), 3758-3779.

12 F. Zhang, Y. H. Deng, Y. F. Shi, R. Y. Zhang and D. Y. Zhao, *J. Mater. Chem.*,

2010, **20**(19), 3895-3900.

13 Y. J. Sun, Y. Chen, L. J. Tian, Y. Yu, X. G. Kong, J. W. Zhao and H. Zhang, *Nanotechnology*, 2007, **18**(27), 275609.

14 J. H. Zeng, J. Su, Z. H. Li, R. X. Yan and Y. D. Li, *Adv. Mater.*, 2005, **17**(17), 2119-2123.

15 G. S. Yi, H. C. Lu, S. Y. Zhao, Y. Ge, W. J. Yang, D. P. Chen and L. H. Guo, *Nano Lett.*, 2004, **4**(11), 2191-2196.

16 J. C. Boyer, F. Vetrone, L. A. Cuccia and J. A. Capobianco, *J. Am. Chem. Soc.*, 2006, **128**(23), 7444-7445.

17 H. S. Qian and Y. Zhang, *Langmuir*, 2008, **24**(21), 12123-12125.

18 Y. Wei, F. Q. Lu, X. R. Zhang and D. P. Chen, *Chem. Mater.*, 2006, **18**(24), 5733-5737.

19 L. Cheng, C. Wang and Z. Liu, *Nanoscale*, 2013, **5**(1), 23-37.

20 Y. M. Yang, Q. Shao, R. R. Deng, C. Wang, X. Teng, K. Cheng, Z. Cheng, L. Huang, Z. Liu, X. G. Liu and B. G. Xing, *Angew. Chem. Int. Ed.*, 2012, **51**(13), 3125-3129.

21 T. Y. Cao, Y. Yang, Y. Gao, J. Zhou, Z. Q. Li, F. Y. Li, *Biomaterials*, 2011, **32**(11), 2959-2968

22 G. Tian, Z. J. Gu, L. J. Zhou, W. Y. Yin, X. X. Liu, L. Yan, S. Jin, W. L. Ren, G. M. Xing, S. J. Li and Y. L. Zhao, *Adv. Mater.*, 2012, **24**(9), 1226-1231

23 D. M. Yang, X. J. Kang, P. A. Ma, Y. L. Dai, Z. Y. Hou, Z. Y. Cheng, C. X. Li, J. Lin, *Biomaterials*, 2013, **34**(5), 1601-1602.

24 Z. Q. Li, Y. Zhang and S. Jiang, *Adv. Mater.*, 2008, **20**(24), 4765-4769.

25 N. Lang and A. Tuel, *Chem. Mater.*, 2004, **16**(10), 1961-1966.

26 H. X. Mai, Y. W. Zhang, L. D. Sun and C. H. Yan, *J. Phys. Chem. C.*, 2007, **111**(37), 13721-13729.

27 N. J. J. Johnson, N. M. Sangeetha, J. C. Boyer and F. C. van Veggel, *Nanoscale*, 2010, **2**(5), 771-777.

28 C. X. Li, Z. Y. Hou, Y. L. Dai, D. M. Yang, Z. Y. Cheng, P. A. Ma and J. Lin, *Biomater. Sci.*, 2013, **1**(2), 213-223.

29 J. P. Yang, Y. H. Deng, Q. L. Wu, J. Zhou, H. F. Bao, Q. Li, F. Zhang, F. Y. Li, B. Tu and D. Y. Zhao, *Langmuir*, 2010, **26** (11), 8850-8856.

30 C. X. Li, J. L. Liu, S. Alonso, F. Y. Li and Y. Zhang, *Nanoscale*, 2012, **4**(19), 6065-6071.

31 S. J. Zhang, Z. X. Jiang, X. H. Liu, L. P. Zhou and W. J. Peng, *Nanoscale*, 2013, **5**(17), 8146-8155.

32 P. P. Yang, S. L. Gai and J. Lin, *Chem. Soc. Rev.*, 2012, **41**(9), 3679-3698.

33 J. Shi, Z. Hua and L. Zhang, *J. Mater. Chem.*, 2004, **14**(5), 795-806.

34 Q. He, X. Cui, F. Cui, L. Guo and J. Shi, *Microporous and Mesoporous Mater.*, 2009, **117**(3), 609-616.

35 G. Tian, W. Y. Yin, J. J. Jin, X. Zhang, G. M. Xing, S. J. Li, Z. J. Gu and Y. L. Zhao, J. *Mater. Chem. B*, 2013, DOI: 10.1039/C3TB21394C.

Figure captions:

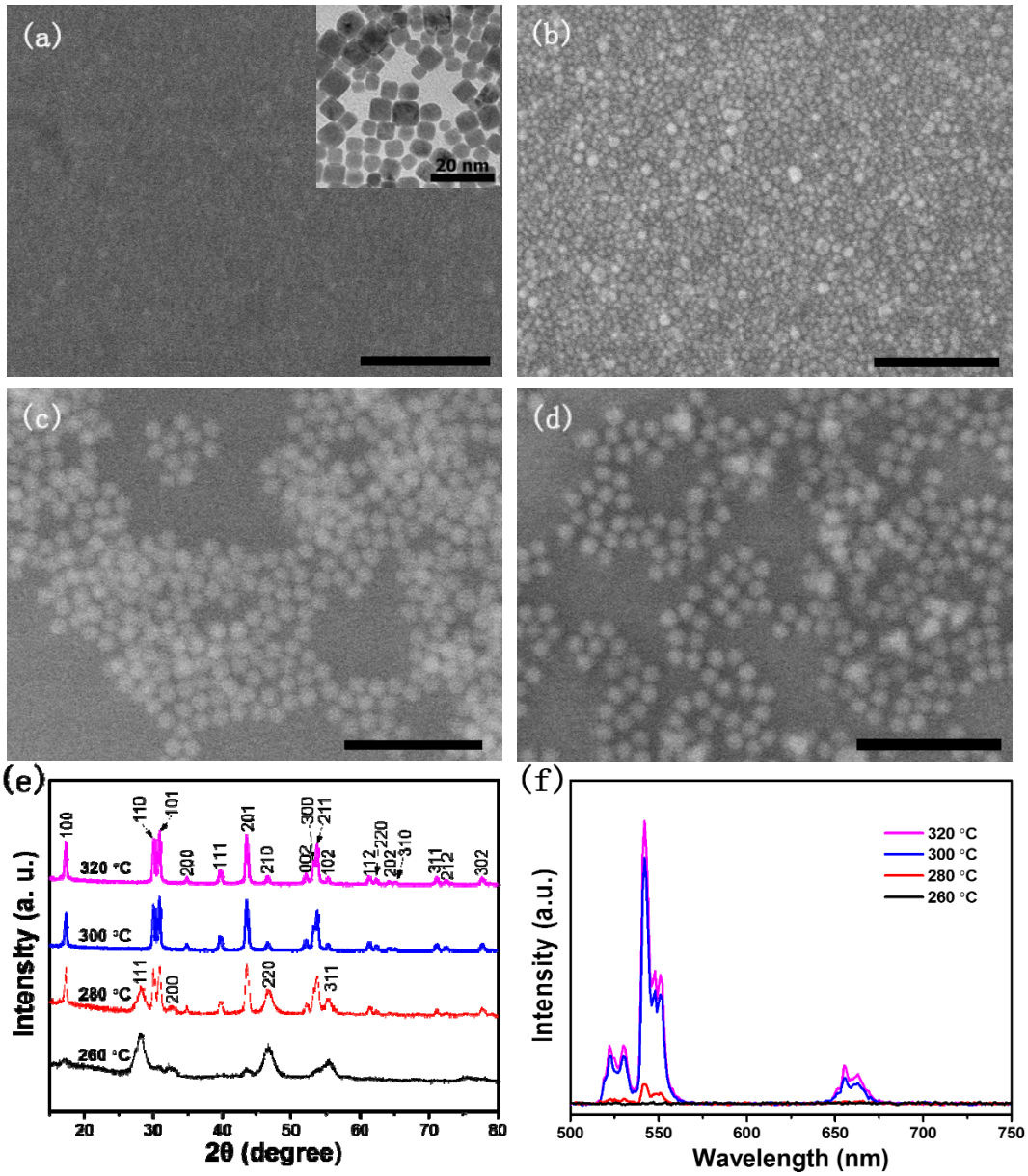

Figure 1. Effect of reaction temperature. SEM images of $NaYF_4$:Yb/Er nanoparticles obtained at different temperatures for 1 h: (a) 260 ºC, (b) 280 ºC, (c) 300 ºC and (d) 320 ºC. All scale bars are 200 nm. Figure 1a inset: the corresponding TEM image. (e) Corresponding XRD patterns and (f) upconversion emission spectrum under 980-nm excitation (1 mg/mL in cyclohexane, laser power: 500 mW).

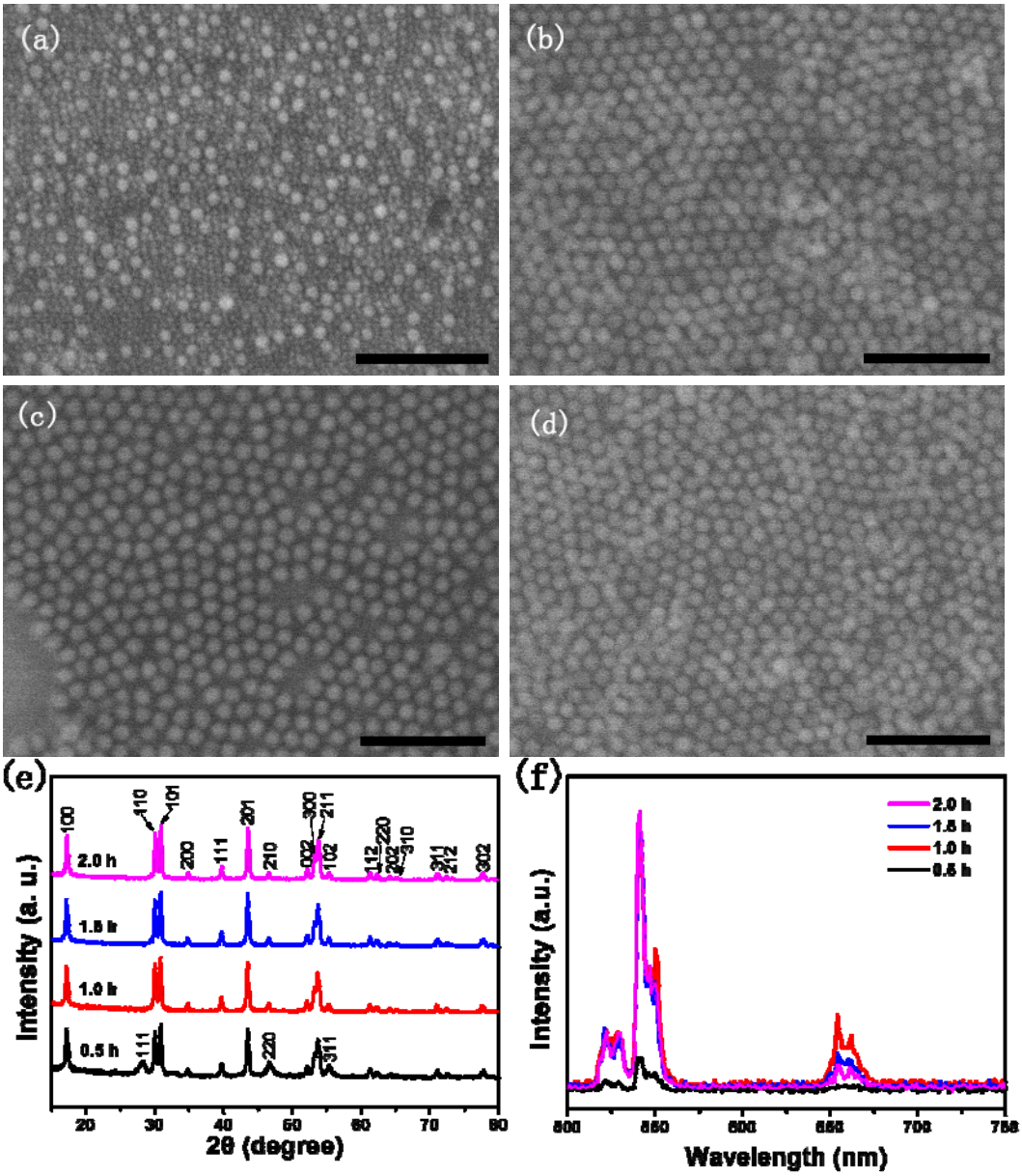

Figure 2. Effect of reaction time. SEM images of $NaYF_4$:Yb/Er nanoparticles obtained at different reaction time at 300 ºC: (a) 0.5 h, (b) 1.0 h, (c) 1.5 h and (d) 2.0 h. All scale bars are 200 nm. (e) Corresponding XRD patterns and (f) upconversion emission spectrum under 980-nm excitation (1 mg/mL in cyclohexane, laser power: 500 mW).

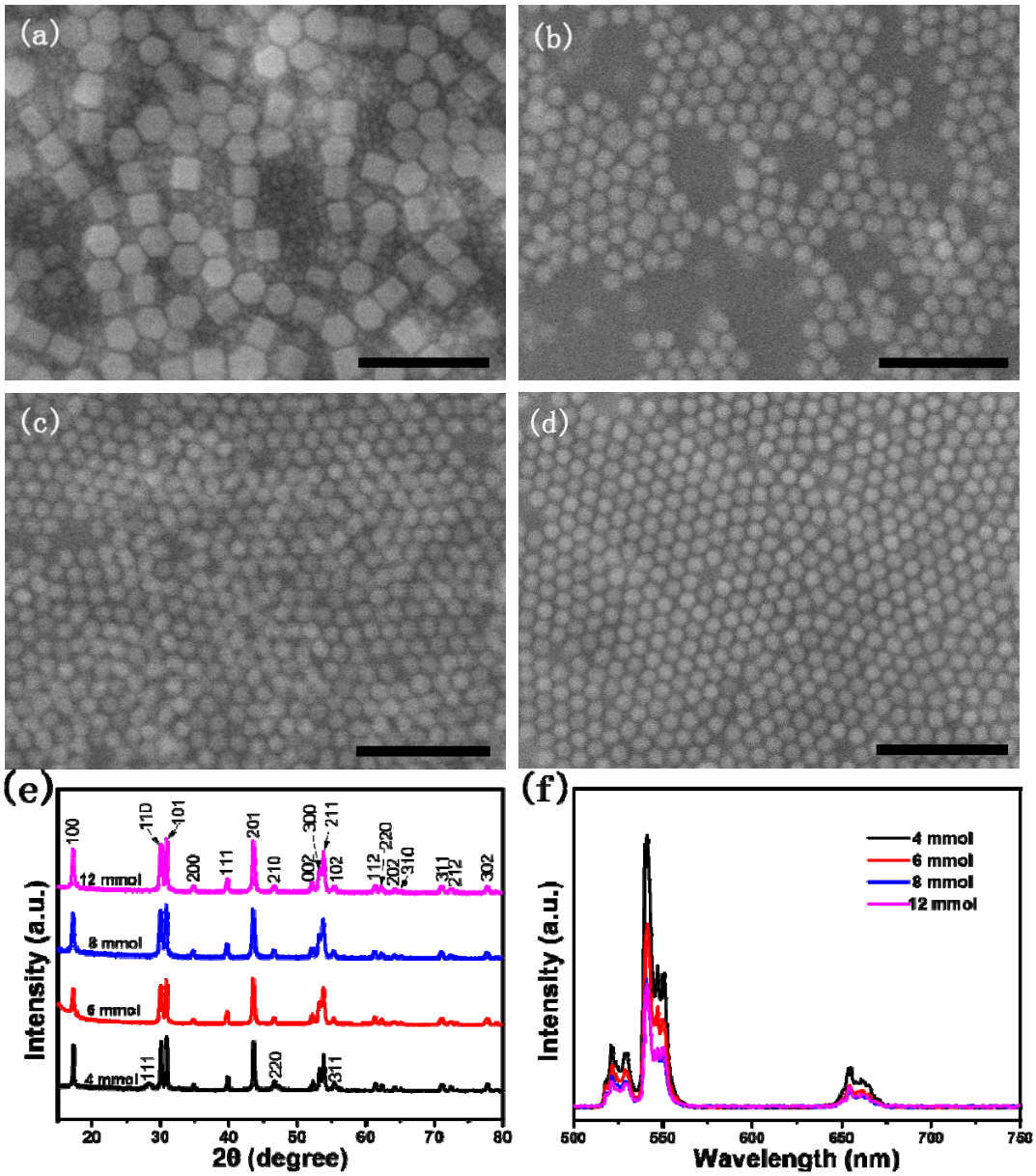

Figure 3. Effect of added NaF amount. SEM images of $NaYF_4$:Yb/Er nanoparticles obtained at different NaF concentrations at 300 ºC for 1 h: (a) 4 mmol, (b) 6 mmol, (c) 8 mmol and (d) 12 mmol. All scale bars are 200 nm. (e) Corresponding XRD patterns and (f) upconversion emission spectra under 980-nm excitation (1 mg/mL in cyclohexane, laser power: 500 mW).

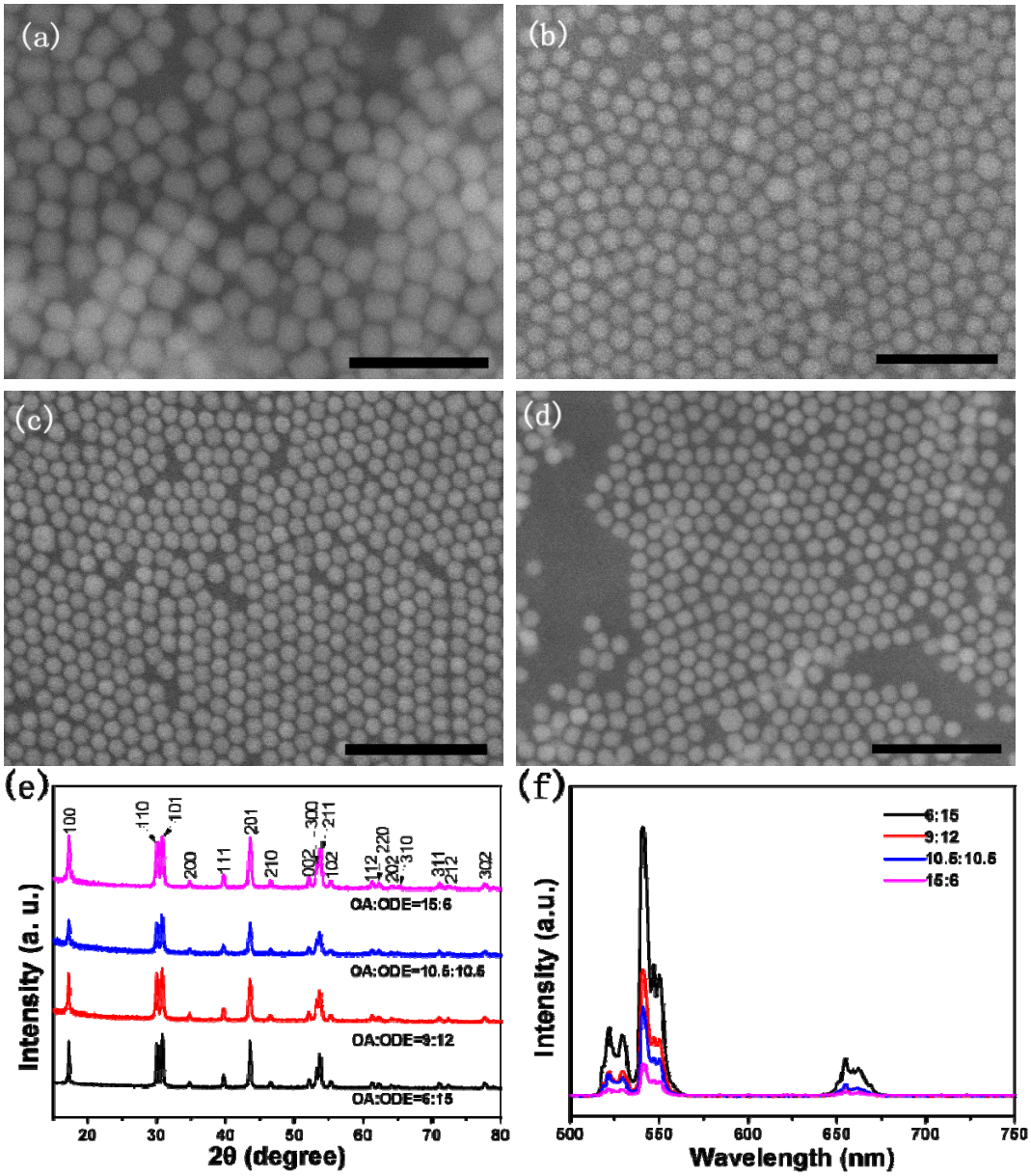

Figure 4. Effect of the ligand. SEM images of $NaYF_4$:Yb/Er nanoparticles obtained at different oleic acid concentrations at 300 ºC for 1 h: (a) 6 mL, (b) 9mL, (c) 10.5 mL and (d) 15 mL. All scale bars are 200 nm. (e) Corresponding XRD patterns and (f) upconversion emission spectrum under 980-nm excitation (1 mg/mL in cyclohexane, laser power: 500 mW).

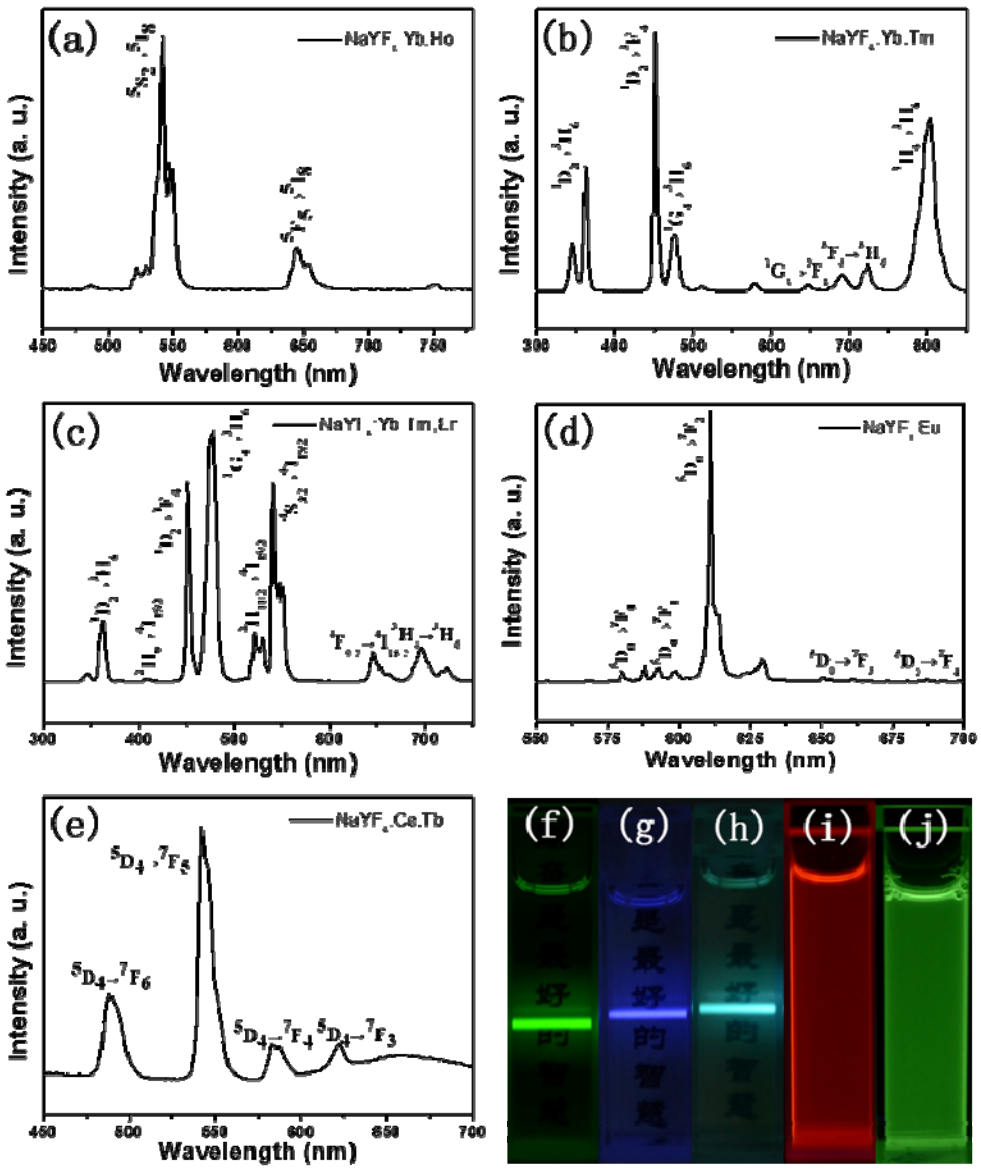

Figure 5. Multicolor UC and DC luminescence. UC emission spectrum of $NaYF_4$ nanoparticles doped with (a) Yb/Ho (20/2 mol%), (b) Yb/Tm (20/0.2 mol%) and Yb/Tm/Er (20/0.5/0.2 mol%) dispersed in cyclohexane (1 mg/mL) under 980-nm excitation. DC fluorescence spectra of $NaYF_4$:Eu (5 mol%) and $NaYF_4$:Ce/Tb (20/5 mol%) dispersed in cyclohexane (1 mg/mL) under 254-nm UV irradiation. (f-j) Corresponding luminescent images. UCL images (f) (j) and (h) corresponding to spectra (a), (b) and (c), respectively, were collected under 500 mW 980-nm irradiation with 3s exposure time; DC images (i) and (j) corresponding to spectra (d) and (e), respectively, were taken at 254 nm with a hand-held UV lamp with 1s exposure time.

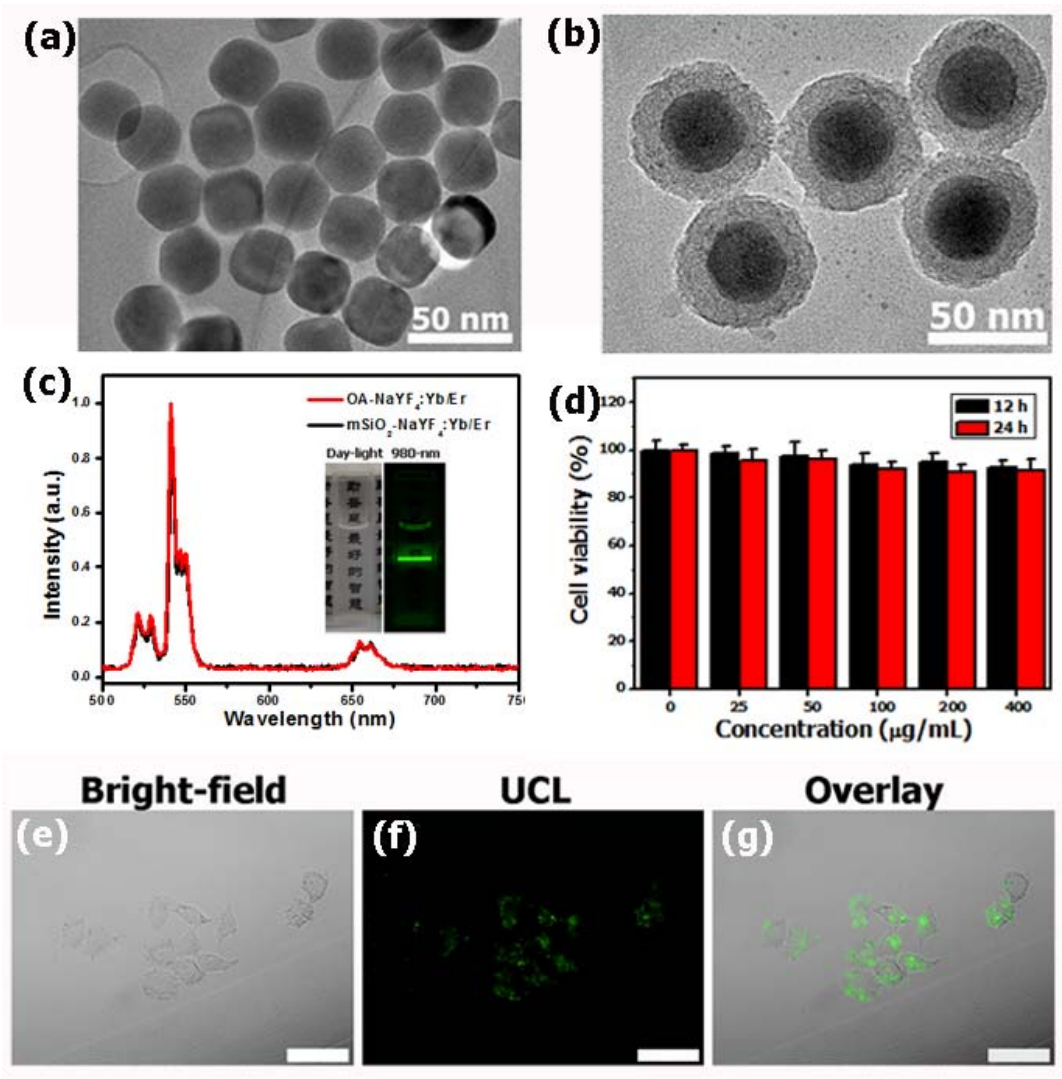

Figure 6. Surface modification and bio-imaging. TEM images of UCNPs (a) before and (b) after being coated with a mesoporous silica layer. (c) UCL spectra of OA-UCNPs dispersed in cyclohexane and $mSiO_2$-$NaYF_4$:Yb/Er dispersed in cyclohexane with same concentration (0.5 mg/mL), respectively. Inset: daylight and UCL images of $mSiO_2$-$NaYF_4$:Yb/Er dispersion (laser power: 500 mW, exposure time: 3 s). (d) Cell viability of HeLa cells incubated with $mSiO_2$-$NaYF_4$:Yb/Er at different concentrations for 24 h and 48 h, respectively. (e-g). In vitro cell imaging performed with inverted microscopy under 980-nm excitation. (e) bright-field image, (f) UCL image, and (g) overlay image of (e) and (f). All scale bars are 50 μm.

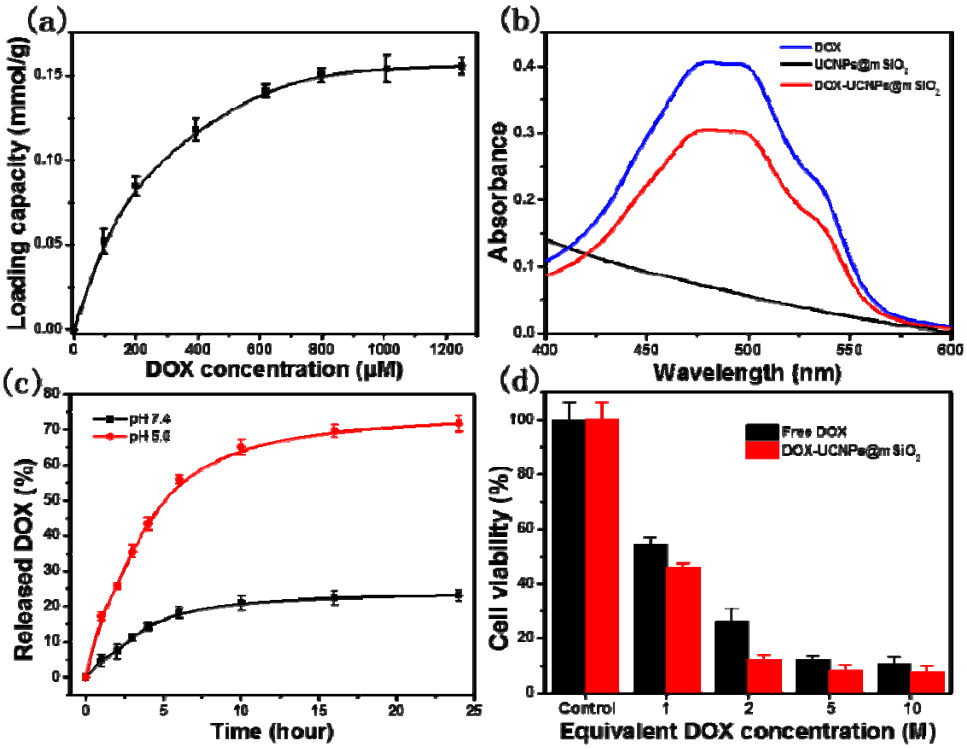

Figure 7. DOX storage/release behavior and cell killing estimation. (a) Quantification of DOX loading at different DOX concentrations. Error bars were based on standard deviations of triplicated samples. (b) UV-vis absorbance spectrum of free DOX, bare UCNPs@mSiO$_2$ and DOX-UCNPs@mSiO$_2$. (c) Real time monitoring DOX release from DOX-UCNPs@mSiO$_2$ in PBS medium at two different pH values. Error bars were based on standard deviations of triplicated samples. (d) Concentration-dependent cell viability of Hela cells cultured with free DOX and DOX-UCNPs@mSiO$_2$.

Table of contents

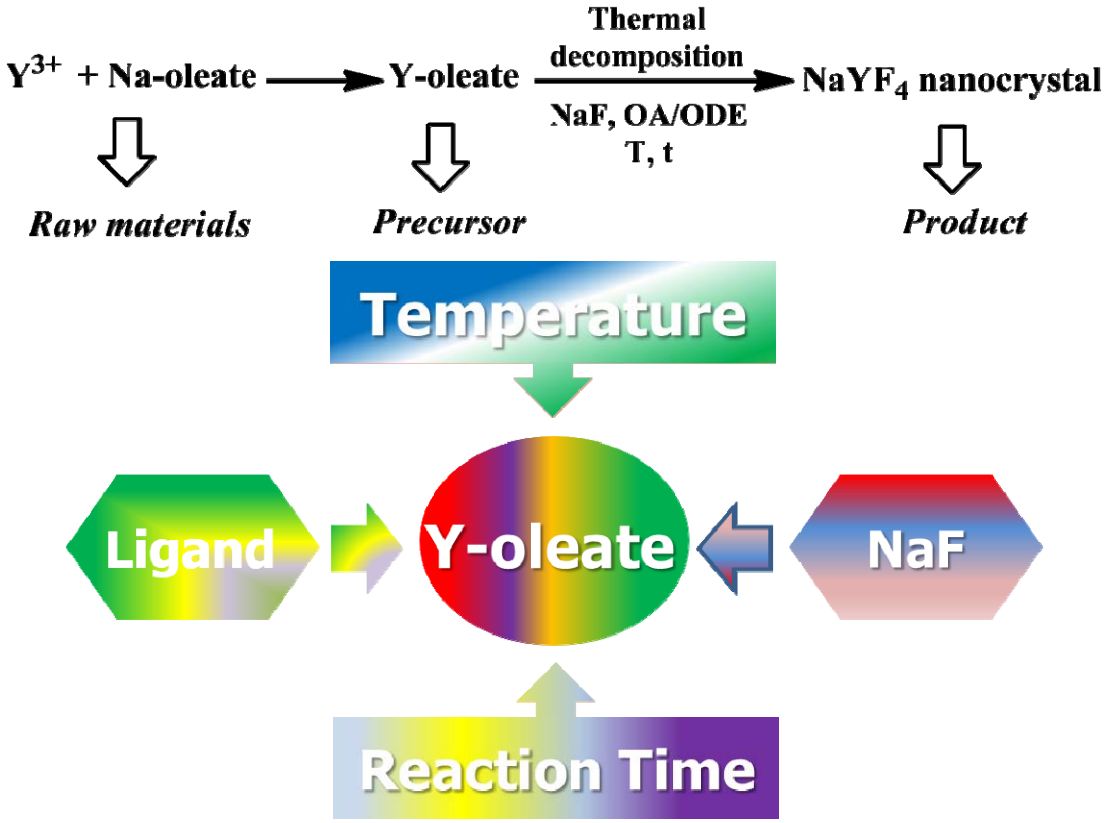

A two-step synthetic rote for fabrication of hexagonal-phase $NaYF_4$ and $NaYF_4$-based nano-phosphors based on thermal decomposition of their corresponding oleate precursors is provided. Influence factors on the morphology, crystal phase and luminescent properties of the final products, such as reaction temperature, time, ligands (OA/ODE ratio) and NaF amount are systematically investigated, indicating the reliability of the proposed strategy and enriching the synthetic route for hexagonal-phase $NaYF_4$.